Separating Partially-Polarized Diffuse and Specular Reflection Components under Unpolarized Light Sources

Soma Kajiyama, Taihe Piao, Ryo Kawahara, and Takahiro Okabe
Department of Artificial Intelligence, Kyushu Institute of Technology
680-4 Kawazu, Iizuka, Fukuoka 820-8502, Japan
{rkawahara, okabe}@ai.kyutech.ac.jp

Abstract

Separating diffuse and specular reflection components observed on an object surface is important for preprocessing of various computer vision techniques. Conventionally, diffuse-specular separation based on the polarimetric and color clues assumes that the diffuse/specular reflection components are unpolarized/partially polarized under unpolarized light sources. However, the diffuse reflection component is partially polarized in fact, because the diffuse reflectance is maximal when the polarization direction is parallel to the outgoing plane. Accordingly, we propose a method for separating partially-polarized diffuse and specular reflection components on the basis of the polarization reflection model and the dichromatic reflection model. In particular, our method enables us not only to achieve diffuse-specular separation but also to estimate the polarimetric properties of the object surface from a single color polarization image. We experimentally confirmed that our method performs better than the method assuming unpolarized diffuse reflection components.

1. Introduction

In general, the reflected light observed on an object surface consists of a diffuse reflection component and a specular reflection component. Separating those reflection components is important for preprocessing of various techniques in computer vision and computer graphics such as multi-view stereo [31], shape from shading [16, 36], shape from polarization [45], relighting [12], and image-based material editing [25, 19].

For diffuse-specular separation, we can make use of the difference in the colors of diffuse and specular reflection components. According to the dichromatic reflection model [32], the color of a specular reflection component is independent of an object surface and is equal to the color of a light source. On the other hand, the color of a diffuse reflection component depends not only on the light source color but also on the spectral reflectance of the object surface. Therefore, the diffuse and specular reflection components can be separated on the basis of the distribution of the observed pixel colors in the RGB color space [18].

We can also make use of the difference in the polarization states of diffuse and specular reflection components. When we observe the reflected light from an object surface illuminated by a polarized light, the specular reflection component is polarized whereas the diffuse reflection component is approximately unpolarized [8]. Therefore, the diffuse and specular reflection components can be separated from the images taken by placing linear polarizers in front of a light source and a camera, and rotating one of them [45].

In order to achieve robust diffuse-specular separation, we can combine the polarimetric and color clues. Nayar *et al*. [26] and Wen *et al*. [43] consider an object illuminated by an unpolarized light source, and separate the diffuse and specular reflection components observed on the object surface under the assumption that the specular reflection component is partially polarized but the diffuse reflection component is *unpolarized*. However, the diffuse reflection component is *partially polarized* in fact. This is because the diffuse reflectance, *i.e.* the Fresnel transmittance coefficient from inside the object, is maximal when the polarization direction is parallel to the outgoing plane spanned by a viewing direction and a surface normal [8]. Therefore, the accuracy of the diffuse-specular separation assuming unpolarized diffuse reflection components is limited.

Accordingly, we propose a method for separating diffuse and specular reflection components on the basis of the polarimetric and color clues under the assumption that both the diffuse and specular reflection components are partially polarized. Our proposed method achieves diffuse-specular separation from a single image taken by using a color polarization camera. Specifically, we formulate the diffuse-specular separation on the basis of the polarization reflection model and the dichromatic reflection model, and esti-

mate the unknowns of the model: the light source color, the diffuse reflection colors, the phase angles, and the degrees of linear polarization (DoLP) for diffuse and specular reflection components. Thus, our method can not only separate diffuse and specular reflection components but also estimate the polarimetric properties of the object surface.

To show the effectiveness of our proposed method, we conducted a number of experiments using both synthetic and real images. We confirmed that our method works well on real images as well as synthetic images, and performs better than the method assuming unpolarized diffuse reflection components.

The main contributions of this study are twofold. First, we propose a novel method for separating partially polarized diffuse and specular reflection components from a single image taken under unpolarized light sources. Compared with the existing methods [26, 43] for diffuse-specular separation based on the polarimetric and color clues, we take partially-polarized diffuse reflection components into consideration. Second, we experimentally confirmed that the proposed method works well for real images and performs better than the method assuming unpolarized diffuse reflection components. In particular, our method enables us not only to separate diffuse and specular reflection components but also to estimate the polarimetric properties of the object surface.

2. Related Work

2.1. Utilizing Color Information

While the color is quite strong information for single-image separation of reflection components, it is insufficient for pixel-wise analytical solution. To overcome this ill-posed problem, various methods with prior knowledge such as the sparsity of specular reflection components have been proposed over the decades since the dichromatic reflection model approach [32] first appeared. Yang *et al*. [47] and Akashi and Okatani [2] designed color-based specular removal as the optimization problems with spatial prior knowledge. Some methods transform the color space in order to use the color information of the entire image [30, 7, 46]. Also as an extended concept, there are methods utilizing specular-free image [38, 37, 48, 33, 34]. Tan *et al*. [38] transformed the image into the maximum chromaticity-intensity space to separate the specular reflection component by using the surrounding diffuse pixels. Although such color space-focused methods are valuable, many of them assume a white light source for robust estimation, and their accuracy is also limited.

2.2. Utilizing Polarimetric Information

Polarization images provide an additional clue to the reflection component separation. Especially in the case that specularly reflected light is fully polarized, the separation becomes quite simple. Thus, the use of fully polarized light sources or a well-tuned setting of incidence and reflection angles can robustly extract the specular reflection component [45, 11, 24, 15, 28, 17, 27, 3]. Realistically, however, the polarization state of the light source is randomly distributed and the specularly reflected light is partially polarized.

Assuming such unpolarized light sources, Nayar *et al*. [26] proposed a method to remove partially polarized specular components by utilizing both color and polarization information. In addition, the color of the light source is estimated from the intensity change of multiple pixels with rotating a linear polarizer in front of the camera. For more robust estimation, Wen *et al*. [43] introduce PCA-based color clustering and optimization with the specular sparsity regularization and implicit function representation of diffuse components. Some other approaches utilize color and polarization information for independent component analysis (ICA) [9, 40, 49, 41]. These studies exploit the difference in polarization states between specular and diffuse reflection components to achieve blind separation by maximizing the independence of those signals.

However, all of the above methods are based on the assumption that diffuse reflection components are unpolarized, which limits their separation accuracy. Moreover, if the separation of the mixtured-polarization state of reflected light is achieved, it would contribute to a number of shape-from-polarization methods [4, 35, 50]. Interestingly, since partially-polarized diffuse reflectance can be modeled as the Fresnel transmittance, the polarization state of the reflected light can be formulated in the same way as those of reflected and transmitted light on transparent surfaces such as glass [29, 20, 44]. On the other hand, these methods differ from ours in the problem setting itself, *i.e.* light sources differ for reflected and transmitted light, and prior information is given for the normals of the transparent surfaces.

Recently, deep learning-based methods using polarization [23, 21, 22, 13] show effective results, but they rely on supervised learning and require large datasets. In contrast, our method achieves the separation of reflection components from a single input image, and also achieves the estimation of the polarimetric properties of the object surface.

3. Reflection Model

Let us consider an object illuminated by a single *unpolarized* light source. In general, the reflected light observed on the object surface consists of specular and diffuse reflection components.

It is well known that the specular reflection component is partially polarized under an unpolarized light source because the specular reflectance depends on the polarization

direction [8]. When we observe the specular reflection component at a surface point through a linear polarizer, the intensity $i_s(\phi)$ is represented as

$$i_s(\phi) = d_s + a_s \cos[2(\phi - \phi_s)]. \quad (1)$$

Here, d_s and a_s are the DC component and the amplitude of the specular reflection component, and ϕ and ϕ_s are the angle of the linear polarizer and the phase angle of the specular reflection. The intensity of the specular reflection component is maximal when $\phi = \phi_s, \phi_s + \pi$. Note that the DoLP for specular reflection ρ_s is given by

$$\rho_s = \frac{a_s}{d_s}. \quad (2)$$

It is often assumed that the diffuse reflection component is unpolarized, but it is weakly polarized in fact, because the diffuse reflectance also depends on the polarization direction [8, 5, 6]. In a similar manner to the specular reflection component, the intensity of the partially polarized diffuse reflection component $i_d(\phi)$ is represented as

$$i_d(\phi) = d_d + a_d \cos[2(\phi - \phi_d)]. \quad (3)$$

Here, d_d and a_d are the DC component and the amplitude of the diffuse reflection component, and ϕ_d is the phase angle of the diffuse reflection. The intensity of the diffuse reflection component is maximal when $\phi = \phi_d, \phi_d + \pi$. Note that the DoLP for diffuse reflection ρ_d is given by

$$\rho_d = \frac{a_d}{d_d}. \quad (4)$$

The specular reflectance, *i.e.* the Fresnel reflectance coefficient, is maximal when the polarization direction is perpendicular to the incoming plane spanned by the light source direction and the surface normal at the point. On the other hand, the diffuse reflectance, *i.e.* the Fresnel transmittance coefficient from inside the object, is maximal when the polarization direction is parallel to the outgoing plane spanned by the viewing direction and the surface normal. For specular reflection components observed on smooth surfaces, the light source direction, the (macroscopic) surface normal, and the viewing direction are coplanar, and then the incoming plane is equal to the outgoing plane. Hence, we assume

$$\phi_d = \phi_s \pm \pi/2. \quad (5)$$

According to the dichromatic reflection model [32], the color of a specular reflection component is independent of an object surface and is equal to the color of a light source. On the other hand, the color of a diffuse reflection component depends not only on the light source color but also on the spectral reflectance of the object surface. We denote the colors (RGB values) of the specular and diffuse reflection components by using 3-D vectors $\boldsymbol{c}_s$ and $\boldsymbol{c}_d$ respectively. Combining those colors and the polarimetric properties in eq.(1), eq.(3), and eq.(5), we can represent the pixel values $\boldsymbol{i}(\phi)$ observed through the linear polarizer with the angle ϕ as

$$\begin{aligned} \boldsymbol{i}(\phi) &= \{d_d - a_d \cos[2(\phi - \phi_s)]\}\boldsymbol{c}_d \\ &+ \{d_s + a_s \cos[2(\phi - \phi_s)]\}\boldsymbol{c}_s. \end{aligned} \quad (6)$$

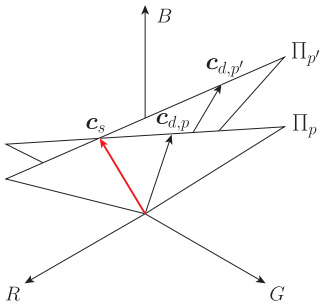

Figure 1. The estimation of a light source color: the intersection of two planes.

4. Proposed Method

4.1. Overview

We consider objects illuminated by a single unpolarized light source or multiple unpolarized light sources with the same color. We assume that the object surfaces are smooth, *i.e.* their surface roughness values are small.

Our proposed method uses a single image taken by using a color polarization camera as input. Such a camera captures scene radiance values through color and linear polarization filters in front of each pixel, and yields 12 radiance values per pixel, *i.e.* 3 color channels (RGB) $\times$ 4 polarization angles ($0°$, $45°$, $90°$, and $135°$). We denote the polarization angle of the camera by ϕ_c $(c = 1, 2, 3, 4)$, and rewrite eq.(6) at the p-th pixel as

$$\begin{aligned} \boldsymbol{i}_p(\phi_c) &= \{d_{d,p} - a_{d,p} \cos[2(\phi_c - \phi_{s,p})]\}\boldsymbol{c}_{d,p} \\ &+ \{d_{s,p} + a_{s,p} \cos[2(\phi_c - \phi_{s,p})]\}\boldsymbol{c}_s. \end{aligned} \quad (7)$$

Note that the light source color $\boldsymbol{c}_s$ is uniform across the image and therefore independent of the pixel p. We explain the details on each step for estimating the unknowns in the following subsections.

4.2. Estimation of Light Source Color

We can see from eq.(7) that the 4 colors observed at each pixel, *i.e.* $\boldsymbol{i}_p(\phi_c)$ $(c = 1, 2, 3, 4)$, are on the plane Π_p spanned by the light source color $\boldsymbol{c}_s$ and the diffuse reflection color $\boldsymbol{c}_{d,p}$ in the RGB color space. Because we assume that the light source color is uniform across the image, the

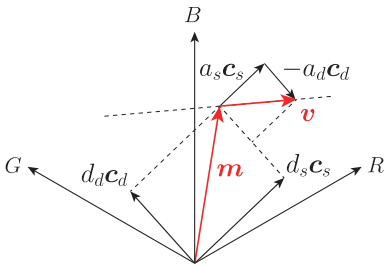

Figure 2. The estimation of a phase angle; the pixel values oscillate around the center $\boldsymbol{m}$ along the direction $\boldsymbol{v}$.

planes obtained at each pixel share the common light source color. Therefore, we can estimate the light source color $\boldsymbol{c}_s$ as the intersection of those planes as shown in Figure 1.

In order to robustly estimate the light source color, we make use of RANdom SAmple Consensus (RANSAC) [14] as follows. First, we compute each plane Π_p spanned by the light source color $\boldsymbol{c}_s$ and the diffuse reflection color $\boldsymbol{c}_{d,p}$ by using SVD. Specifically, we construct 3×4 matrix $\boldsymbol{C}_p$ as

$$\boldsymbol{C}_p = (\boldsymbol{i}_p(\phi_1), \boldsymbol{i}_p(\phi_2), \boldsymbol{i}_p(\phi_3), \boldsymbol{i}_p(\phi_4)), \tag{8}$$

and consider the eigen vector with the smallest eigen value as the normal $\boldsymbol{n}_p$ of the plane Π_p.

Second, we randomly pick up two pixels p' and p'', and then compute the candidate of the light source color $\boldsymbol{c}_s(p', p'')$. Since the light source color is perpendicular to the both normals $\boldsymbol{n}_{p'}$ and $\boldsymbol{n}_{p''}$, the candidate of the light source color is given by the outer product of those normals as

$$\boldsymbol{c}_s(p', p'') = \boldsymbol{n}_{p'} \times \boldsymbol{n}_{p''}. \tag{9}$$

Then, we count the number of inliers; if the angle between the candidate of the light source color and the plane Π_p is less than a threshold t, we consider the plane as an inlier.

Third, we repeat the above step, and find the candidate of the light source color with the maximal number of inliers. Finally, we re-compute the light source color from those inlier planes by using SVD.

4.3. Estimation of Phase Angle

It is easy to estimate the phase angle from gray-scale polarization images. We can fit a cosine curve to the pixel values observed through three polarization angles, *e.g.* $0°$, $45°$, and $90°$, and then estimate the phase angle up to the ambiguity of π. However, the way of estimating the phase angle from color polarization images is not self-evident[1]. For example, the cosine curves fitted to the pixel values of each color channel could have different phase angles due to the noises in pixel values.

[1]The conventional method can be used by converting color images to gray-scale images. However, such estimation is not robust as $\boldsymbol{v}_p$ in eq.(10) is getting perpendicular to $(1, 1, 1)^\top$.

Accordingly, we investigate how the colors observed at each pixel vary according to the polarization angle ϕ_c, and estimate the phase angle $\phi_{s,p}$. We can rewrite eq.(7) as

$$\begin{aligned} \boldsymbol{i}_p(\phi_c) &= [d_{s,p}\boldsymbol{c}_s + d_{d,p}\boldsymbol{c}_{d,p}] \\ &+ [a_{s,p}\boldsymbol{c}_s - a_{d,p}\boldsymbol{c}_{d,p}]\cos[2(\phi_c - \phi_{s,p})] \\ &= \boldsymbol{m}_p + \cos[2(\phi_c - \phi_{s,p})]\boldsymbol{v}_p. \end{aligned} \tag{10}$$

As shown in Figure 2, this equation means that the pixel values oscillate around the center $\boldsymbol{m}_p = d_{s,p}\boldsymbol{c}_s + d_{d,p}\boldsymbol{c}_{d,p}$ along the direction $\boldsymbol{v}_p = a_{s,p}\boldsymbol{c}_s - a_{d,p}\boldsymbol{c}_{d,p}$.

Therefore, we first estimate the direction $\boldsymbol{v}_p$ by fitting a line to the 4 observed colors via least squares. Second, we project the 4 observed colors to the line. Finally, we estimate the phase angle $\phi_{s,p}$ on the basis of the distance between the projected points and the center in a similar manner to the gray-scale polarization image. Note that the estimated phase angle also has the ambiguity of π.

4.4. Estimation of Remaining Unknowns

Since the light source color $\boldsymbol{c}_s$ and the phase angle $\phi_{s,p}$ are estimated in Sections 4.2 and 4.3, we estimate the remaining unknowns in eq.(10). Specifically, combining eq.(10) and eq.(2) and eq.(4), we estimate the 6 unknowns, *i.e.* $\boldsymbol{c}_{d,p}$[2], $d_{s,p}$, $d_{d,p}$, $\rho_{s,p}$, and $\rho_{d,p}$ from

$$\boldsymbol{m}_p = d_{s,p}\boldsymbol{c}_s + d_{d,p}\boldsymbol{c}_{d,p}, \tag{11}$$

$$\boldsymbol{v}_p = \rho_{s,p}d_{s,p}\boldsymbol{c}_s - \rho_{d,p}d_{d,p}\boldsymbol{c}_{d,p}. \tag{12}$$

Note that we can easily obtain the center of oscillation, *i.e.* the DC component $\boldsymbol{m}_p$ by average and the oscillation direction $\boldsymbol{v}_p$ as described in Section 4.3 from the color polarization image.

The number of equations in eq.(11) and eq.(12) is 6 ($= 3 \times 2$). However, the number of linearly independent equations is only 4 ($= 2 \times 2$) in general, because those equations hold on the 2-D plane spanned by $\boldsymbol{c}_s$ and $\boldsymbol{c}_{d,p}$. Since the number of the unknowns is 6, it is clear that the problem of estimating the remaining unknowns is underdetermined, and therefore it is impossible to estimate those unknowns per pixel.

Accordingly, we assume that an object of interest has piece-wise constant albedo and shares the common diffuse reflection color in each region. Specifically, we estimate the remaining unknowns in a region-based manner by nonlinear minimization:

$$\begin{aligned} \min_{\{\boldsymbol{c}_d, d_{s,p}, d_{d,p}, \rho_{s,p}, \rho_{d,p}\}} \sum_{p \in R} \big\{ &[\boldsymbol{m}_p - f(\boldsymbol{c}_d, d_{s,p}, d_{d,p})]^2 \\ &+ [\boldsymbol{v}_p - g(\boldsymbol{c}_d, d_{s,p}, d_{d,p}, \rho_{s,p}, \rho_{d,p})]^2 + w||\nabla\rho_{d,p}|| \big\}. \end{aligned} \tag{13}$$

[2]The degree of freedom of $\boldsymbol{c}_{d,p}$ is 2, because we normalize it so that $c_{d,p1} + c_{d,p2} + c_{d,p3} = 1$.

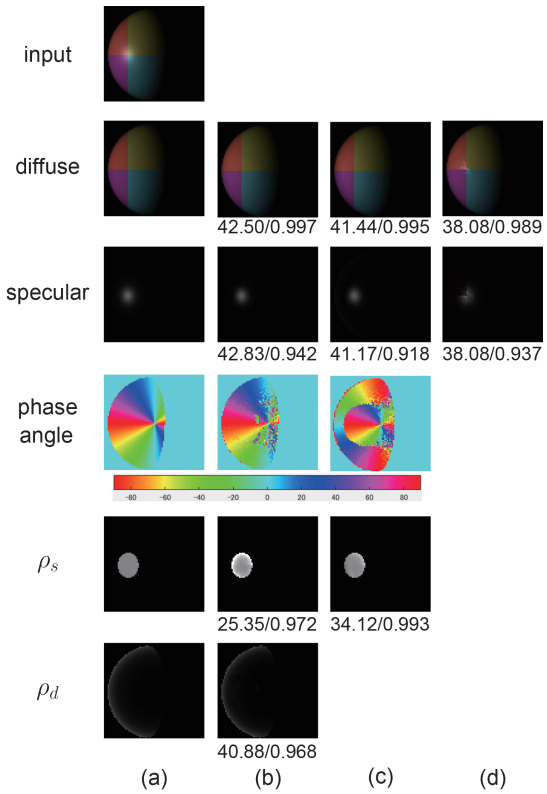

Figure 3. The results on the synthetic image of the 1st scene (a sphere under a single white light source): (a) the ground truth, (b) our proposed method (the polarized diffuse), (c) the unpolarized diffuse, and (d) the only color.

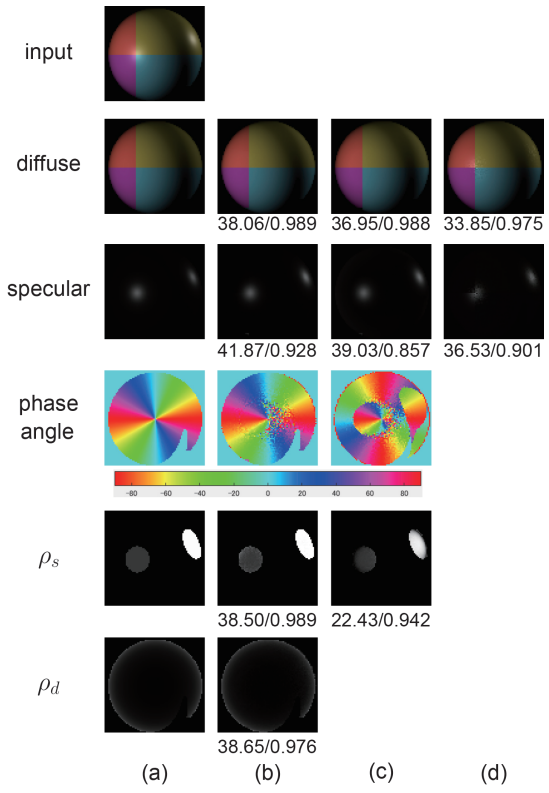

Figure 4. The results on the synthetic image of the 2nd scene (a sphere under two white light sources): (a) the ground truth, (b) our proposed method (the polarized diffuse), (c) the unpolarized diffuse, and (d) the only color.

Here, the functions f and g in the first and second terms are the right-hand sides of eq.(11) and eq.(12) respectively, and w is the weight for balancing the first and second terms and the third term. Since the DoLP of diffuse reflection components varies smoothly on an object surface, we add the third term, *i.e.* the total variation regularization with respect to the DoLP of diffuse reflection components. Please see Appendix for the details on the optimization.

5. Experiments

To confirm the effectiveness of our proposed method, we conducted a number of experiments using both synthetic and real images. We compared the performance of the following three methods:

- **Polarized Diffuse**: our proposed method assuming partially-polarized diffuse reflection components.
- **Unpolarized Diffuse**: the method assuming the unpolarized diffuse reflection components. It assumes $a_{d,p} = 0$ in eq.(7), and then estimates the unknowns other than $a_{d,p}$ in a similar manner to our method for direct comparison.
- **Only Color**: the existing method [2] for diffuse-specular separation from a single color image for reference. The input color image is given by averaging a color polarization image with respect to the polarization angles.

We used the trust-region algorithm [10] implemented as lsqcurvefit in MATLAB for solving the constrained nonlinear minimization problem of eq.(13). In order to compute the initial values as described in Appendix, we used the SLIC superpixel segmentation [1] implemented as superpixels in MATLAB. We empirically set the threshold for classifying inliers in Section 4.2 as $t = 3°$, and the weight in eq.(13) as $w = 10^{-4}$. The computational cost of the RANSAC-based estimation of a light source color is low; it took about 1 sec for 3,000 random samples (iterations) on an ordinary PC.

5.1. Synthetic Images

We conducted a number of experiments using synthetic images for which all the ground truths are available. We tested four cases: an object with a simple shape (sphere) illuminated by (i) a single white light source and (ii) two

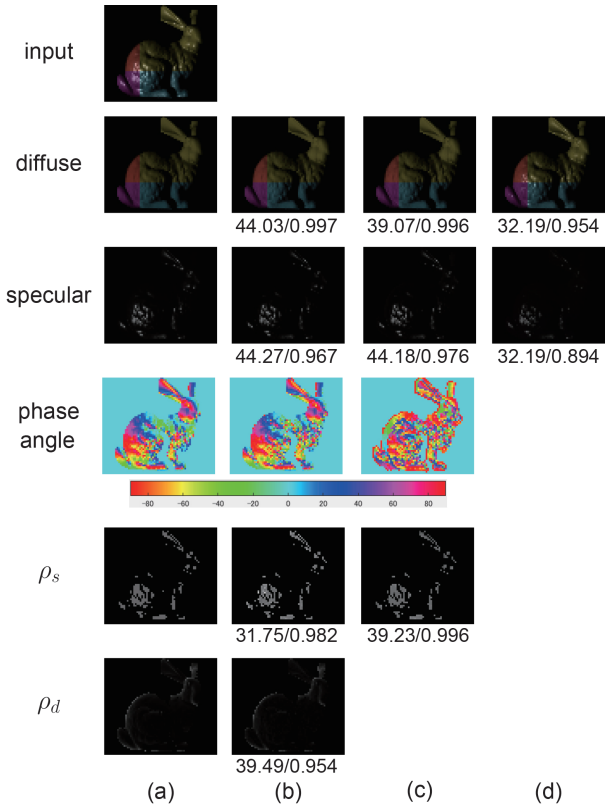

Figure 5. The results on the synthetic image of the 3rd scene (the Stanford Bunny under a single white light source): (a) the ground truth, (b) our proposed method (the polarized diffuse), (c) the unpolarized diffuse, and (d) the only color.

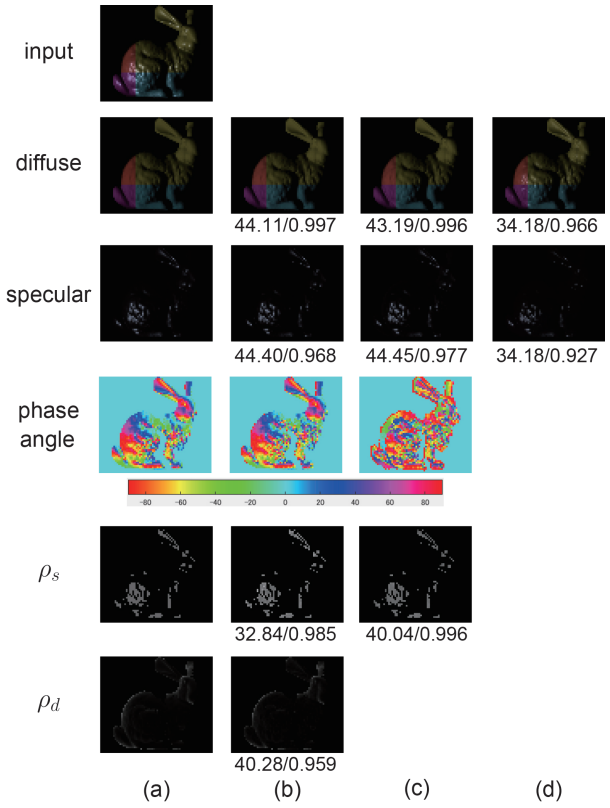

Figure 6. The results on the synthetic image of the 4th scene (the Stanford Bunny under a single bluish light source): (a) the ground truth, (b) our proposed method (the polarized diffuse), (c) the unpolarized diffuse, and (d) the only color.

Table 1. The light source colors: the ground truths, the colors estimated by using our method, and the angular errors in degree.

case	ground truth	estimated	error
(i)	(1/3,1/3,1/3)	(0.334,0.333,0.333)	0.06°
(ii)	(1/3,1/3,1/3)	(0.333,0.334,0.333)	0.09°
(iii)	(1/3,1/3,1/3)	(0.334,0.333,0.333)	0.03°
(iv)	(0.301,0.321,0.378)	(0.301,0.321,0.378)	0.07°

white light sources, and an object with a complex shape (the Stanford Bunny) illuminated by (iii) a single white light source and (iv) a single bluish light source. We added random noises to the synthesized images; we assume photon shot noises, *i.e.* Gaussian noises whose variance σ^2 is proportional to a pixel value [39]. We determined the proportional coefficient so that the total amount of noises is equal to that of the zero-mean Gaussian noises with $\sigma = 0.01$ for pixel values normalized to [0,1].

First, Figure 3 shows the result for (i) a sphere under a single white light source: the input image, the diffuse and specular reflection components, the phase angle, and the DoLPs for specular and diffuse reflection components from top to bottom. We show the ground truths in (a), and the results obtained by using the polarized diffuse, the unpolarized diffuse, and the only color in (b), (c), and (d) respectively. The numerical values under each result image show the PSNRs (Peak Signal-to-Noise Ratios)/SSIMs (Structural Similarity Index Measure) [42]; the higher the better. The color bar shows the phase angle $[-\pi/2, \pi/2]$.

Comparing the results of the diffuse-specular separation, we can see that our proposed method (the polarized diffuse) performs better than the unpolarized diffuse and the only color both qualitatively and quantitatively. Both the polarized diffuse and the unpolarized diffuse enable us to estimate the polarimetric properties of the object surface. We can see that the phase angle $\phi_s (= \phi_d \pm \pi/2)$ estimated by using the unpolarized diffuse flip when the dominant polarization component changes from specular reflection to diffuse reflection. This is because the unpolarized diffuse considers the observed polarized components as specular reflection components. On the other hand, the phase angle estimated by using the polarized diffuse is almost the same as the ground truth, although the results are a little noisy when DoLP is small. We can also see that the polar-

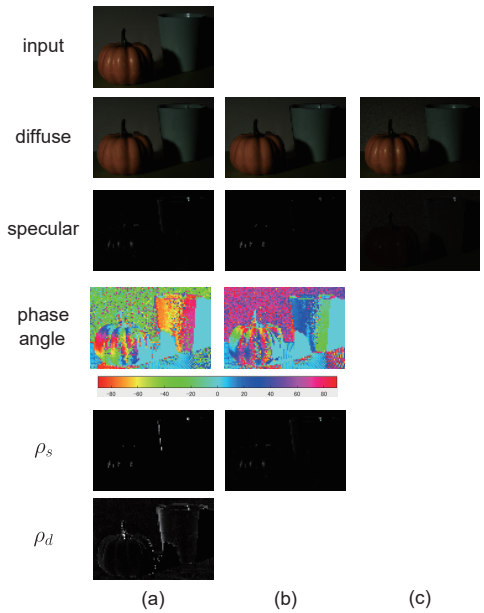

Figure 7. The results on the real image of the scene (A) (a plastic pumpkin and a plastic cup): (a) our proposed method (the polarized diffuse), (b) the unpolarized diffuse, and (c) the only color.

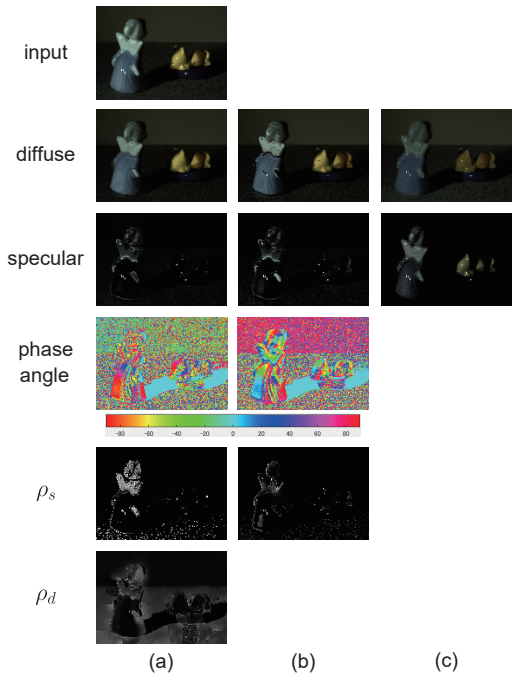

Figure 8. The results on the real image of the scene (B) (ceramic figurines): (a) our proposed method (the polarized diffuse), (b) the unpolarized diffuse, and (c) the only color.

ized diffuse works well for estimating the DoLPs for diffuse and specular reflection components. The unpolarized diffuse performs better for estimating ρ_s, but it cannot estimate ρ_d by definition.

Second, we show the result for (ii) a sphere under two white light sources in Figure 4. We can see from the ground truths of ρ_s and ρ_d that both the DoLPs for diffuse and specular reflection components have large values at the same location, *i.e.* the upper right area of the sphere under those light sources. Similar to the first case, we can see that our proposed method (the polarized diffuse) performs better than the unpolarized diffuse and the only color. In particular, our method works better than the unpolarized diffuse when both the DoLPs for diffuse and specular reflection components have large values at the same location.

Third, we show the result for (iii) the Stanford Bunny under a single white light source in Figure 5. Similar to the first and second cases, we can see that our proposed method (the polarized diffuse) performs better than the unpolarized diffuse and the only color also for an object with a complex shape.

Forth, we show the result for (iv) the Stanford Bunny under a single bluish light source in Figure 6. Similar to the previous cases, we can see that our proposed method (the polarized diffuse) performs better than the unpolarized diffuse and the only color also for a non-white light source.

Table 1 summarizes the light source colors: the ground truths, the colors estimated by using our method, and the angular errors between them in degree. We can see that our method can accurately estimate the light source colors.

5.2. Real Images

We conducted a number of experiments using real images. We tested three scenes: (A) a plastic pumpkin and a plastic cup, (B) ceramic figurines, and (C) a plastic sphere and a plastic holder. The images of those scenes were captured by using a color polarization camera BFS-U3-51S5PC-C from FLIR. Here, the ground truths other than the light source colors are unknown[3]; we measured the light source color by directly capturing the emitted light with the same camera and considered it as the ground truth.

Figure 7, Figure 8, and Figure 9 show the results for the scenes (A), (B), and (C). We show the results obtained by using our proposed method (the polarized diffuse), the unpolarized diffuse, and the only color in (a), (b), and (c) respectively. Comparing the results of the diffuse-specular separation, we can see that our method performs better than the unpolarized diffuse and the only color qualitatively. We can see that the phase angles estimated by using the polarized diffuse and the unpolarized diffuse are noisy in dark areas, but our method performs better than the unpolarized diffuse because most of the estimated phase angles flip due

[3]In contrast to conventional evaluation, we cannot consider the variable components observed through a rotating linear polarizer as specular components because diffuse components are also partially-polarized and variable.

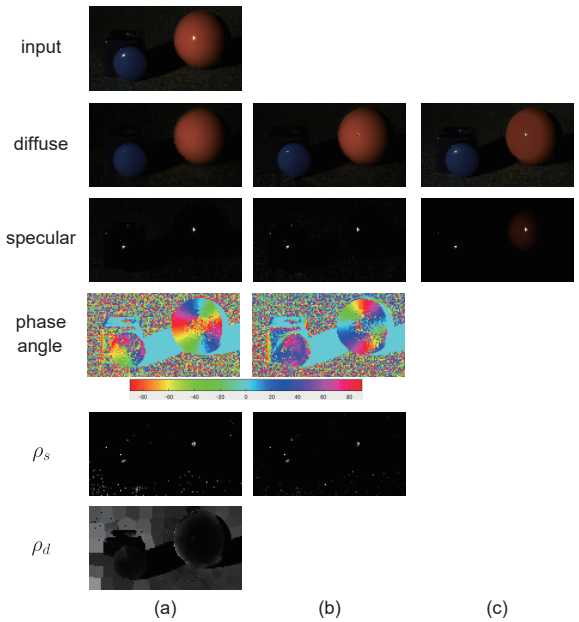

Figure 9. The results on the real image of the scene (C) (a plastic sphere and a plastic holder): (a) our proposed method (the polarized diffuse), (b) the unpolarized diffuse, and (c) the only color.

Table 2. The light source colors: the ground truths, the colors estimated by using our method, and the angular errors in degree.

scene	ground truth	estimated	error
(A)	(0.308,0.360,0.331)	(0.310,0.360,0.330)	0.23°
(B)	(0.308,0.360,0.331)	(0.307,0.361,0.332)	0.16°
(C)	(0.308,0.360,0.331)	(0.319,0.349,0.332)	1.52°

to the assumption of unpolarized diffuse reflection components. In addition, similar to the experimental results on synthetic images we can see that our method can recover the DoLP for diffuse reflection components near the occluding contours of objects.

Table 2 summarizes the light source colors: the ground truths, the colors estimated by using our method, and the angular errors between them in degree. We can see that our method can accurately estimate the light source colors.

6. Conclusion and Future Work

In this paper, we proposed a method for separating diffuse and specular reflection components on the basis of the polarization reflection model and the dichromatic reflection model. In particular, we assume that both the diffuse and specular reflection components are partially polarized under unpolarized light sources, and achieve the estimation of the polarimetric properties of the object surface as well as the diffuse-specular separation from a single color polarization image. We experimentally confirmed that our proposed method performs better than the method assuming unpolarized diffuse reflection components.

The extension to fully or partially polarized light sources is one of the directions of our future study. Another direction is the CV applications such as shape from polarization and image-based material editing.

Acknowledgement: This work was supported by JSPS KAKENHI Grant Numbers JP20H00612 and JP21K21319.

A. Optimization

We optimize eq.(13) via alternative least squares. Specifically, we segment the input image into the regions with approximately the same diffuse reflection colors, and estimate the initial values for $\boldsymbol{c}_d$ per region and those for $d_{s,p}$, $d_{d,p}$, $\rho_{s,p}$, and $\rho_{d,p}$ per pixel as follow. Then, we repeatedly update $\boldsymbol{c}_d$ and $\{d_{s,p}, d_{d,p}, \rho_{s,p}, \rho_{d,p}\}$ in turn until convergence.

First, we compute a rough specular-free image by assuming that the diffuse reflection components are unpolarized and the specular reflection components are fully polarized. Then, we segment the input color image on the basis of the normalized colors of the specular-free image by using one of the existing methods for image segmentation. We consider the median of the diffuse reflection components over each region as $\boldsymbol{c}_d$.

Second, we compute the initial values for $d_{s,p}$ and $d_{d,p}$ on the basis of eq.(11). Specifically, we assume that both $\boldsymbol{c}_s$ and $\boldsymbol{c}_d$ are given, we compute the initial values by solving

$$\boldsymbol{m}_p = d_{s,p}\boldsymbol{c}_s + d_{d,p}\boldsymbol{c}_d \tag{14}$$

via least squares. Here, we impose the non-negative constraints: $d_{s,p} \geq 0$ and $d_{d,p} \geq 0$, because the DC components of the diffuse and specular reflection components are non-negative.

Third, in a similar manner to the above, we compute the initial values for $\rho_{s,p}$ and $\rho_{d,p}$ on the basis of eq.(12). Because the phase angle estimated in Section 4.3 has the ambiguity of π, we compute the initial values of $a_{s,p}$ and $a_{d,p}$by solving

$$\pm\boldsymbol{v}_p = a_{s,p}\boldsymbol{c}_s - a_{d,p}\boldsymbol{c}_d \tag{15}$$

via least squares subject to the non-negative constraints: $a_{s,p} \geq 0$ and $a_{d,p} \geq 0$. Then, we select the solution with the smaller squared errors as the initial values for $a_{s,p}$ and $a_{d,p}$. Finally, we convert them to $\rho_{s,p}$ and $\rho_{d,p}$ from eq.(2) and eq.(4).

References

[1] R. Achanta, A. Shaji, K. Smith, A. Lucchi, P. Fua, and S. Süsstrunk. Slic superpixels compared to state-of-the-art superpixel methods. *IEEE TPAMI*, 34(11):2274–2282, 2012.

[2] Y. Akashi and T. Okatani. Separation of reflection components by sparse non-negative matrix factorization. In *Proc. ACCV2014*, pages 611–625, 2014.

[3] K. Arieda and T. Okabe. Illumination planning for measuring per-pixel surface roughness. In *Proc. IAPR MVA2021*, pages 1–5, 2021.

[4] G. Atkinson and E. Hancock. Recovery of surface orientation from diffuse polarization. *IEEE TIP*, 15(6):1653–1664, 2006.

[5] S.-H. Baek, D. Jeon, X. Tong, and M. Kim. Simultaneous acquisition of polarimetric SVBRDF and normals. *ACM TOG*, 37(6):268:1–15, 2018.

[6] S.-H. Baek, T. Zeltner, H. Ku, I. Hwang, X. Tong, W. Jakob, and M. Kim. Image-based acquisition and modeling of polarimetric reflectance. *ACM TOG*, 39(4):139:1–14, 2020.

[7] R. Bajcsy, S.-W. Lee, and A. Leonardis. Detection of diffuse and specular interface reflections and inter-reflections by color image segmentation. *IJCV*, 17(3):241–272, 1996.

[8] M. Born and E. Wolf. *Principles of Optics*. Pergamon Press, 1959.

[9] A. Bronstein, M. Bronstein, M. Zibulevsky, and Y. Zeevi. Sparse ICA for blind separation of transmitted and reflected images. *International Journal of Imaging Systems and Technology*, 15(1):84–91, 2005.

[10] T. Coleman and Y. Li. An interior, trust region approach for nonlinear minimization subject to bounds. *SIAM Journal on Optimization*, 6:418–445, 1996.

[11] O. Cula, K. Dana, D. Pai, and D. Wang. Polarization multiplexing and demultiplexing for appearance-based modeling. *IEEE TPAMI*, 29(2):362–367, 2007.

[12] P. Debevec, T. Hawkins, C. Tchou, H.-P. Duiker, W. Sarokin, and M. Sagar. Acquiring the reflectance field of a human face. In *Proc. ACM SIGGRAPH2000*, pages 145–156, 2000.

[13] V. Deschaintre, Y. Lin, and A. Ghosh. Deep polarization imaging for 3D shape and SVBRDF acquisition. In *Proc. IEEE/CVF CVPR2021*, pages 15567–15576, 2021.

[14] M. Fischler and R. Bolles. Random sample consensus: A paradigm for model fitting with applications to image analysis and automated cartography. *Commun. ACM*, 24(6):381–395, 1981.

[15] A. Ghosh, G. Fyffe, B. Tunwattanapong, J. Busch, X. Yu, and P. Debevec. Multiview face capture using polarized spherical gradient illumination. In *Proc. ACM SIGGRAPH2011*, pages 1–10, 2011.

[16] B. Horn. *Obtaining Shape from Shading Information*, pages 123–171. MIT Press, 1989.

[17] L. Jospin, G. Baechler, and A. Scholefield. Embedded polarizing filters to separate diffuse and specular reflection. In *Proc. ACCV2018*, pages 3–18, 2018.

[18] G. Klinker, S. Shafer, and T. Kanade. A physical approach to color image understanding. *IJCV*, 4:7–38, 1990.

[19] N. Kobayashi and T. Okabe. Separating reflection components in images under multispectral and multidirectional light sources. In *Proc. IAPR ICPR2016*, pages pp.3199–3204, 2016.

[20] N. Kong, Y.-W. Tai, and J. Shin. A physically-based approach to reflection separation: from physical modeling to constrained optimization. *IEEE TPAMI*, 36(2):209–221, 2013.

[21] C. Lei, X. Huang, M. Zhang, Q. Yan, W. Sun, and Q. Chen. Polarized reflection removal with perfect alignment in the wild. In *Proc. IEEE CVPR2020*, pages 1750–1758, 2020.

[22] R. Li, S. Qiu, G. Zang, and W. Heidrich. Reflection separation via multi-bounce polarization state tracing. In *Proc. ECCV2020*, pages 781–796, 2020.

[23] Y. Lyu, Z. Cui, S. Li, M. Pollefeys, and B. Shi. Reflection separation using a pair of unpolarized and polarized images. In *Proc. NeurIPS2019*, volume 32, 2019.

[24] W.-C. Ma, T. Hawkins, P. Peers, C.-F. Chabert, M. Weiss, and P. Debevec. Rapid acquisition of specular and diffuse normal maps from polarized spherical gradient illumination. In *Proc. EGSR2007*, pages 183–194, 2007.

[25] S. Mallick, T. Zickler, P. Belhumeur, and D. Kriegman. Specularity removal in images and videos: a PDE approach. In *Proc. ECCV2006*, number I, pages 550–563, 2006.

[26] S. Nayar, X.-S. Fang, and T. Boult. Separation of reflection components using color and polarization. *IJCV*, 21:163–186, 1997.

[27] Y. Nisaka, R. Matsuoka, T. Amano, and T. Okabe. Fast separation of specular, diffuse, and global components via polarized pattern projection. In *Frontiers of Computer Vision (Proc. IW-FCV2021)*, pages 294–308, 2021.

[28] J. Riviere, I. Reshetouski, L. Filipi, and A. Ghosh. Polarization imaging reflectometry in the wild. *ACM TOG*, 36(6):206:1–14, 2017.

[29] Y. Schechner, J. Shamir, and N. Kiryati. Polarization-based decorrelation of transparent layers: The inclination angle of an invisible surface. In *Proc. IEEE ICCV'99*, volume 2, pages 814–819, 1999.

[30] K. Schlüns and M. Teschner. Fast separation of reflection components and its application in 3D shape recovery. In *Proc. Color Imaging Conference 1995*, pages 48–51, 1995.

[31] S. Seitz, B. Curless, J. Diebel, D. Scharstein, and R. Szeliski. A comparison and evaluation of multi-view stereo reconstruction algorithms. In *Proc. IEEE CVPR2006*, pages 2402–2409, 2006.

[32] S. Shafer. Using color to separate reflection components. *COLOR Research and Application*, 10(4):210–218, 1985.

[33] H.-L. Shen and Q.-Y. Cai. Simple and efficient method for specularity removal in an image. *Applied Optics*, 48(14):2711–2719, 2009.

[34] H.-L. Shen and Z.-H. Zheng. Real-time highlight removal using intensity ratio. *Applied Optics*, 52(19):4483–4493, 2013.

[35] W. Smith, R. Ramamoorthi, and S. Tozza. Linear depth estimation from an uncalibrated, monocular polarization image. In *Proc. ECCV2016*, pages 109–125, 2016.

[36] K. Takechi and T. Okabe. Diffuse-specular separation of multi-view images under varying illumination. In *Proc. IEEE ICIP2017*, pages 2632–2636, 2017.

[37] R. Tan and K. Ikeuchi. Separating reflection components of textured surfaces using a single image. In *Digitally Archiving Cultural Objects*, pages 353–384. 2008.

[38] R. Tan, K. Nishino, and K. Ikeuchi. Separating reflection components based on chromaticity and noise analysis. *IEEE TPAMI*, 26(10):1373–1379, 2004.

[39] Y. Tsin, V. Ramesh, and T. Kanade. Statistical calibration of CCD imaging process. In *Proc. IEEE ICCV2001*, pages 480–487, 2001.

[40] S. Umeyama and G. Godin. Separation of diffuse and specular components of surface reflection by use of polarization and statistical analysis of images. *IEEE TPAMI*, 26(5):639–647, 2004.

[41] F. Wang, S. Ainouz, C. Petitjean, and A. Bensrhair. Specularity removal: A global energy minimization approach based on polarization imaging. *CVIU*, 158:31–39, 2017.

[42] Z. Wang, A. Bovik, H. Sheikh, and E. Simoncelli. Image quality assessment: from error visibility to structural similarity. *IEEE TIP*, 13(4):600–612, 2004.

[43] S. Wen, Y. Zheng, and F. Lu. Polarization guided specular reflection separation. *IEEE TIP*, 30:7280–7291, 2021.

[44] P. Wieschollek, O. Gallo, J. Gu, and J. Kautz. Separating reflection and transmission images in the wild. In *Proc. ECCV2018*, 2018.

[45] L. Wolff and T. Boult. Constraining object features using a polarization reflectance model. *IEEE TPAMI*, 13(7):635–657, 1991.

[46] J. Yang, L. Liu, and S. Li. Separating specular and diffuse reflection components in the hsi color space. In *Proc. IEEE ICCV2013 Workshops*, pages 891–898, 2013.

[47] Q. Yang, S. Wang, and N. Ahuja. Real-time specular highlight removal using bilateral filtering. In *Proc. ECCV2010*, pages 87–100, 2010.

[48] K.-J. Yoon, Y. Choi, and I.-S. Kweon. Fast separation of reflection components using a specularity-invariant image representation. In *Proc. IEEE ICIP2006*, pages 973–976, 2006.

[49] L. Zhang, E. Hancock, and G. Atkinson. Reflection component separation using statistical analysis and polarisation. In *IbPRIA*, 2011.

[50] D. Zhu and W. Smith. Depth from a polarization + rgb stereo pair. In *Proc. IEEE CVPR2019*, pages 7586–7595, 2019.